Photofragment alignment in the photodissociation of I_2 from 450 to 510 nm

D. A. Chestakov and D. H. Parker[a)]
University of Nijmegen, Toernooiveld 1, 6525 ED Nijmegen, The Netherlands

K. V. Vidma
Institute of Chemical Kinetics and Combustion, Instituskaja Strasse 3, Novosibirsk 630090, Russia

T. P. Rakitzis
Institute of Electronic Structure and Laser, Foundation for Research and Technology-Hellas, 711 10 Heraklion-Crete, Greece

(Received 26 August 2005; accepted 9 November 2005; published online 11 January 2006)

A combination of velocity map imaging and slicing techniques have been used to measure the product recoil anisotropy and angular momentum polarization for the photodissociation process $I_2 \rightarrow I(^2P_{3/2}) + I(^2P_{3/2})$ and $I_2 \rightarrow \dot{I}(^2P_{3/2}) + I(^2P_{1/2})$ in the 450–510 nm laser wavelength region using linearly polarized photolysis and probe laser light. The former channel is produced predominantly via perpendicular excitation to the $^1\Pi_u$ state, and the latter is predominantly parallel, via the $B\,^3\Pi(0_u)^+$ state. In both cases we observe mostly adiabatic dissociation, which produces electronically aligned iodine atoms in the $|m|=1/2$ states with respect to the recoil direction.
© *2006 American Institute of Physics*. [DOI: 10.1063/1.2147203]

I. INTRODUCTION

Vector correlations in photodissociation, particularly the $[\varepsilon, v, J]$ three-vector correlation where ε is the photodissociation laser polarization direction, v the product recoil velocity, and J the product angular momentum vector, have attracted the interest of molecular physicists for many years.[1] Recently, they have been studied with renewed vigor since the complete quantum-mechanical description of Siebbeles *et al.*,[2] and due to the experimental advances in imaging techniques. Important information about the dissociation dynamics, the shape of the potential curves, the symmetries of the excited states, and the role of nonadiabatic interactions can be obtained from a detailed analysis of the photofragment recoil anisotropy and angular momentum polarization[2–8]

Photofragment vector correlations have been measured using velocity map ion imaging,[9,10] Doppler profiles,[11] and ion time-of-flight profiles.[12,13] The most recent and robust technique is the direct measurement of the photofragment polarization using slice imaging,[14,15] where a narrow "slice" through the middle of the sphere of recoiling ionized photofragments is detected, allowing the direct measurement of the angular distribution of this sphere without the need for any deconvolution procedure. The power of the method is demonstrated in this paper on molecular iodine, which plays an active role in atmospheric photochemistry because of its chemical and spectroscopic properties.

Mulliken conducted the first detailed theoretical studies of the I_2 molecule and summarized the results of previous works in his seminal paper.[16] Since then, many experimental papers have been published on the topic.[17–27] Tellinghuisen made some of the most significant contributions[22–26] to the I_2 spectroscopic studies. The vacuum-ultraviolet absorption spectrum of I_2,[18,19] Rydberg states, ion-pair states, and autoionizing Rydberg states of I_2 have inspired recent research.[26,28,29] While $[\varepsilon, v, J]$ measurements have provided information on nonadiabatic processes in the photodissociation of the Cl_2 and Br_2 molecules[30] and the interhalogens IBr,[31] ICl, and BrCl, similar data is not yet available for I_2. Asano and Yabushita[32] have recently presented theoretical predictions for I_2 which are examined in this paper.

We present here the measurements of alignment and orientation of ground-state $I(^2P_{3/2})$ atoms following dissociation of the I_2 molecule to the first and second dissociation limits. The I-atom laboratory-frame polarization data is converted to the molecular-frame polarization parameters $a_q^{(k)}(p)$, where the index p distinguishes between contributions to the photofragment polarization from parallel ($\parallel$) or perpendicular ($\perp$) transitions, or mixed transitions ($\parallel, \perp$).

Some of the known potential-energy surfaces of I_2 are shown schematically in Fig. 1. The ground state of I_2 is of $^1\Sigma_g^+(0_g^+)$ symmetry, where the value of Ω is given in parentheses. Many of the low-lying excited states of I_2 can be

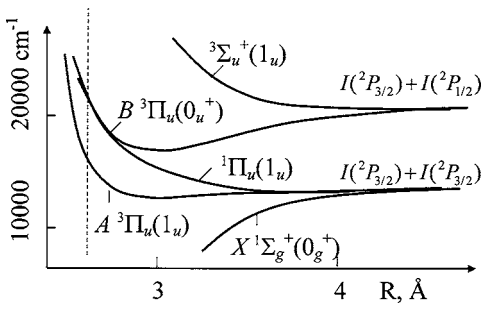

FIG. 1. Potential-energy curves of the I_2 molecule that participate in the dissociation process studied here.

[a)]Author to whom correspondence should be addressed. Electronic mail: parker@science.ru.nl

accessed via fully allowed ($\Delta\Omega=0,\pm1, g\rightarrow u, +\rightarrow+$) one-photon transitions from the ground state in the visible-infrared range. The purely continuum absorption spectrum of molecular iodine ranges from 400 to 499 nm, mainly due to transitions to the $^1\Pi_u(1_u)$ and $B\,^3\Pi(0_u)^+$ states. The continuum region is followed by bound transitions to the $B\,^3\Pi(0_u)^+$ state and continuous absorption to the $^1\Pi_u$ state between 499 and 840 nm. Absorption to the $A\,^3\Pi_{1u}(1_u)$ state starts at 540 nm and becomes dominant above 650 nm.[33] Our studies cover photodissociation in the 510–450 nm region.

II. EXPERIMENT

A brief overview of our velocity map imaging setup, which has been described in detail elsewhere, is given here. A pulsed valve creates a molecular beam of I_2 vapor (0.2 Torr) in argon (2 bars). The molecular beam passes a 2 mm skimmer into the ion lens system where the first dye laser (0.1–0.2 mJ/pulse, collimation diameter ~2 mm, and pulse duration ~6 ns) dissociates the iodine molecules, and the iodine atoms recoil with a fixed amount of excess energy. After about 10–20 ns, a second dye laser pulse (0.3 mJ/pulse, focused by an $f=25$ cm lens, and pulse duration ~6 ns) ionizes the iodine atoms from the ground $^2P_{3/2}$ state through the $^4P_{1/2}$ intermediate state by (2+1) resonantly enhanced multiphonon ionization (REMPI) at 303.68 nm (vacuum wavelength). The polarization of both lasers can be chosen to be either linear or circular. The recoiling ions fly apart, forming an ion sphere. After 1500 ns the electric field of the ion lens is switched on in the velocity mapping mode[15] and the ions are accelerated towards a two-dimensional (2D) position-sensitive multichannel plate (MCP) detector able to detect single ions. The MCP detector is gated by a homebuilt high-voltage pulse supply with $\tau_{\text{pulse}}\sim25$ ns. This short-time gate of the detector allows selective detection of only the middle slice of the ion sphere. The MCP detector, combined with a phosphor screen, converts each single ion event into a light spot. A charge-coupled device (CCD) camera records the ion image from the phosphor screen, and a personal computer (PC) accumulates and stores the image for further analysis. The image contains information about the product recoil anisotropy and polarization from the angular distribution and the product kinetic energy from the radial distribution.

For the image analysis, we follow Rakitzis and Zare and write (in the molecular frame) the relative probability I to ionize iodine atoms after dissociation of the I_2 molecule,

$$\begin{aligned} I[\Theta,\Phi,\theta_\varepsilon,\beta,a_q^{(k)}(p)] &= 1+\beta P_2(\cos\theta_\varepsilon)+s_1G_1\sqrt{2}\sin\theta_\varepsilon\cos\theta_\varepsilon\sin\Theta\sin\Phi\,\mathrm{Im}[a_1^{(1)}(\parallel,\perp)] \\ &+ s_2G_2\{(1+\beta)\cos^2\theta_\varepsilon P_2(\cos\Theta)a_0^{(2)}(\parallel)+(1-\beta/2)\sin^2\theta_\varepsilon P_2(\cos\Theta)a_0^{(2)}(\perp) \\ &+ \sqrt{3/2}\sin\theta_\varepsilon\cos\theta_\varepsilon\sin2\Theta\cos\Phi\,\mathrm{Re}[a_1^{(2)}(\parallel,\perp)]+\sqrt{3/2}(1-\beta/2)\sin^2\Theta\cos2\Phi a_2^{(2)}(\perp)\}, \end{aligned} \tag{1}$$

where Θ is the angle between the recoil direction and polarization axis $\boldsymbol{\varepsilon}_{\text{probe}}$ of detection laser, Φ is the angle between the projections of $\boldsymbol{\varepsilon}_{\text{probe}}$ and $\boldsymbol{\varepsilon}_{\text{phot}}$ onto the plane perpendicular to the detection axis, θ_ε is the angle between photolysis laser polarization and recoil direction, and $P_2(x)$ is the Legendre polynomial of second order. Sensitivity factors s_1 and s_2 depend explicitly on the ellipticity of the detection laser polarization and the particular REMPI scheme used. Hyperfine depolarization coefficients G_1 and G_2 account for electronic depolarization[34] due to the coupling between the iodine nuclear spin and the electronic angular momentum. Using Eqs. (9a)–(9d) from Rakitzis *et al.*,[35] we can transform Eq. (1) to the laboratory frame for all experimental geometries. The result of such transformation can in general be represented in the following form:

$$\begin{aligned} I^{XY}(\theta) &= b_0^{(XY)}+b_1^{(XY)}P_1(\cos\theta)+b_2^{(XY)}P_2(\cos\theta) \\ &+ b_3^{(XY)}P_3(\cos\theta)+b_4^{(XY)}P_4(\cos\theta), \end{aligned} \tag{2}$$

where b_k are the coefficients that depend on the polarization parameters, XY denotes the polarization directions of the *dissociation* and *detection* lasers, respectively, and $P_k(x)$ is a Legendre polynomial of k order. Numerical values of b_k can be found by fitting the experimental angular distributions by using Eq. (2). In our experiment, only even k-member parameters were measured, thus b_0, b_2, and b_4. General expressions for these b_k in the case of $J=3/2$ for some geometries of XY are

$$b_0^{(VV)} = 1-\frac{G_2s_2}{15}((2-\beta)a_0^2(\perp)-2(1+\beta)a_0^{(2)}(\parallel)), \tag{3a}$$

$$\begin{aligned} b_2^{(VV)} &= \beta+\frac{G_2s_2}{21}((2-\beta)[5a_0^{(2)}(\perp)-4\sqrt{6}a_2^{(2)}(\perp)] \\ &+ 11(1+\beta)a_0^{(2)}(\parallel)+2\sqrt{6}\,\mathrm{Re}(a_1^{(2)}(\parallel,\perp))), \end{aligned} \tag{3b}$$

$$\begin{aligned} b_4^{(VV)} &= \frac{2G_2s_2}{35}(-(2-\beta)[\sqrt{6}a_2^{(2)}(\perp)+3a_0^{(2)}(\perp)] \\ &+ 6(1+\beta)a_0^{(2)}(\parallel)-4\sqrt{6}\,\mathrm{Re}[a_1^{(2)}(\parallel,\perp)]), \end{aligned} \tag{3c}$$

$$\begin{aligned} b_0^{(VH)} &= 1-\frac{G_2s_2}{6}((2-\beta)[a_0^{(2)}(\perp)+\sqrt{6}a_2^{(2)}(\perp)] \\ &+ (1+\beta)a_0^{(2)}(\parallel)), \end{aligned} \tag{3d}$$

TABLE I. Polarization parameters for $I(^2P_{3/2})$ products of I_2 photodissociation to the $I(^2P_{3/2})+I(^2P_{3/2})$ channel.

	510 nm	509 nm	490 nm	481.67 nm	468.33 nm	451.34 nm
β	−0.88±0.03	−0.93±0.02	−0.93±0.03	−0.93±0.03	−0.93±0.02	−0.94±0.02
$a_0^{(2)}(\perp)$	−0.58±0.22	−0.85±0.08	−0.58±0.13	−0.86±0.16	−0.60±0.09	−0.68±0.04
$a_2^{(2)}(\perp)$	−0.01±0.16	−0.14±0.12	0.00±0.04	0.12±0.18	−0.05±0.07	−0.05±0.07
$\mathrm{Re}[a_1^{(2)}]$	−0.14±0.03	−0.07±0.04	−0.18±0.02	−0.16±0.05	−0.14±0.02	−0.04±0.22
$P(J=3/2, m_L=\pm 1/2)$	0.86±0.14	1.00±0.05	0.86±0.08	1.00±0.09	0.87±0.06	0.92±0.02

$$b_2^{(VH)} = \beta + \frac{G_2 s_2}{6}((2-\beta)[a_0^{(2)}(\perp) + \sqrt{6}a_2^{(2)}(\perp)] - 2(1+\beta)a_0^{(2)}(\parallel)), \tag{3e}$$

$$b_0^{(HV)} = \frac{G_2 s_2}{12}(2-\beta)(6 + 3a_0^{(2)}(\perp) - \sqrt{6}a_2^{(2)}(\perp)), \tag{3f}$$

$$b_2^{(HV)} = -\frac{G_2 s_2}{6}(2-\beta)(3a_0^{(2)}(\perp) + \sqrt{6}a_2^{(2)}(\perp)), \tag{3g}$$

where V and H signify the linear laser polarization lying parallel or orthogonal to the detector face, respectively. These equations are limited by $k \leqslant 2$ members only, since numerical coefficients for the $k=3$ parameters are relatively small.

For (2+1) REMPI detection of atomic iodine from the $^2P_{3/2}$ state through the $^4P_{1/2}$ intermediate state with linear polarized light, $s_1=0$ and $s_2=-5/4$. For circularly polarized probe light, $s_1=-9/\sqrt{15}$ and $s_2=5/4$. Hyperfine depolarization coefficients can be calculated [Eq. (87), Chap. 5, Ref. 34] and for iodine atoms with $J=3/2$ and nuclear spin $I=5/2$ they are $G_1=173/432$ and $G_2=1957/8400$. After substitution into Eqs. (3a)–(3g) it is possible to solve numerically the set of equations in order to find all of the polarization parameters. The obtained parameters are presented in Tables I and II, with error bars obtained by the varying of the experimental values of b_k in fitting expressions (3a)–(3g).

III. RESULTS AND DISCUSSION

A typical raw experimental image is shown in Fig. 2, where two (large radius) perpendicular and several (small radius) parallel channels are clearly resolved. The parallel dissociation channels are formed by the dissociation process $I_2[X(v=0,1,2,3,\ldots)] \xrightarrow{450\text{–}510\ \mathrm{nm}} I(^2P_{3/2})+I(^2P_{1/2})$ from the different vibrational states of $I_2(X)$ ground state in the molecular beam. Our method resolves the small vibrational energy spacing of 214.5 cm^{-1} for dissociation near threshold. By comparing the relative intensities of these channels and accounting for the Franck-Condon factors for transitions from each particular $I_2(X)$ vibrational state to the B state, we find a vibrational temperature of I_2 in the molecular beam of 240±10 K, which is typical for vibrational cooling in a supersonic beam. The rotational temperature is estimated to be much lower; a value of ~5 K is typical for our conditions.

For the perpendicular channels the signals from different vibrational states are not resolved because the kinetic-energy resolution reduces with increasing fragment energy in velocity space. The smaller-radius perpendicular channel arises from $I_2[X(v=0,1,2,3,\ldots)] \xrightarrow{450\text{–}510\ \mathrm{nm}} I(^2P_{3/2})+I(^2P_{3/2})$. The outermost channel is formed by probe laser photons only: $I_2[X(v=0,1,2,3,\ldots)] \xrightarrow{304\ \mathrm{nm}} I(^2P_{3/2})+I(^2P_{3/2})$. The sharpness of the outer channels of the image shown in Fig. 2 is reduced by distortion due to the finite size of the ion lens system. This distortion is easily avoided by making the image smaller, using a higher electrostatic lens voltage, as shown in the inset in Fig. 2. Table I contains the extracted polarization parameters for the $(I\ ^2P_{3/2}+I\ ^2P_{3/2})$ channel following photodissociation at 450–510 nm, using *VV* and *VH* laser geometries. Selected data from Tables I and II are shown graphically in Fig. 3.

The excited electronic states that participate in the dissociation, the $^1\Pi_u(1_u)$, $B\ ^3\Pi(0_u)^+$, and $A\ ^3\Pi_u(1_u)$ states, correlate asymptotically to the atomic m states $|m_A, m_B\rangle$ as

$$|\pm 1_u\rangle_{^1\Pi_u} \xrightarrow{R\to\infty} \left|\pm\tfrac{1}{2}, \pm\tfrac{1}{2}\right\rangle, \tag{4}$$

$$|\pm 1_u\rangle_A \xrightarrow{R\to\infty} \frac{1}{\sqrt{2}}\left(\left|\pm\tfrac{3}{2}, \mp\tfrac{1}{2}\right\rangle + \left|\mp\tfrac{1}{2}, \pm\tfrac{3}{2}\right\rangle\right), \tag{5}$$

TABLE II. Polarization parameters for $I(^2P_{3/2})$ products of I_2 photodissociation to the $I(^2P_{3/2})+I(^2P_{1/2})$ channel, and v is the vibration quantum numbers of I_2.

	490 nm[a]			481.67 nm[a]				
	$v=0$	$v=1$	$v=2$	$v=0$	$v=1$	$v=2$	468.33 nm	451.34 nm
β	1.85±0.05	1.92±0.08	1.58±0.12	1.95±0.05	1.95±0.05	1.95±0.05	1.85±0.05	0.85±0.05
$a_0^{(2)}(\parallel)$	−0.65±0.07	−0.75±0.05	−0.67±0.13	−0.6±0.2	−0.65±0.15	−0.75±0.05	−0.57±0.09	−0.7±0.1
$a_0^{(2)}(\perp)$	−0.75±0.05	−0.76±0.08	−0.46±0.34	−0.51±0.3	−0.54±0.26	−0.65±0.15	−0.46±0.17	−0.65±0.26
$a_2^{(2)}(\perp)$	0.22±0.17	0.27±0.30	0.16±0.50	0.16±0.34	−0.03±0.20	−0.11±0.14	−0.02±0.20	−0.24±0.27
$\mathrm{Re}[a_1^{(2)}]$	0.18±0.06	0.21±0.14	0.05±0.50	0.05±0.36	0.27±0.21	0.33±0.36	−0.03±0.01	−0.13±0.12

[a]Vibrational resolution was possible here.

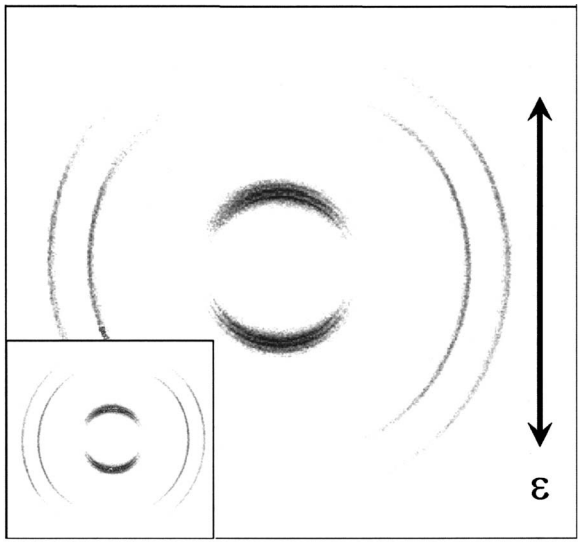

FIG. 2. Raw iodine $I(^2P_{3/2})$ image taken at a dissociation laser wavelength of 451.34 nm with the *VV* experimental geometry. The laser polarization direction ε is indicated along the vertical axis of the image and darker regions correlate with higher signal levels. The initial vibrational states of I_2 molecule are clearly resolved in the middle set of rings. Images taken using the *VH* experimental geometry differ only slightly in shape and intensity from the shown *VV* image. The inset shows an image taken with a higher ion lens voltage. The size of the image is smaller but the distortion of the largest rings is avoided.

$$|0_u\rangle_B \xrightarrow{R\to\infty} \frac{1}{\sqrt{2}}\left(\left|+\tfrac{1}{2},-\tfrac{1}{2}\right\rangle+\left|-\tfrac{1}{2},+\tfrac{1}{2}\right\rangle\right). \tag{6}$$

The values of the $a_0^{(2)}$ parameter (for $J=3/2$) can be written in terms of the difference between the m-state populations $p(m)$ of the $|m|=3/2$ and $|m|=1/2$ states,[36]

$$a_0^{(2)} = \tfrac{4}{5}[p(|m|=3/2) - p(|m|=1/2)], \tag{7}$$

so that the $a_0^{(2)}$ parameter ranges from $+4/5$ (for all the population in the $|m|=3/2$ states) to $-4/5$ (for all the population in the $|m|=1/2$ states), and is 0 for equal population of the $|m|=3/2$ and $|m|=1/2$ states.

We consider the first dissociation channel (Table I and Fig. 3), which yields two ground-state iodine atoms,

$$I_2 \xrightarrow{h\upsilon} I(^2P_{3/2}) + I(^2P_{3/2}). \tag{8}$$

This channel is produced predominantly by perpendicular excitation (notice that β is close to -1) from the ground state to the $^1\Pi_u$ state. In this case, for adiabatic dissociation described by Eq. (4), we see that the $I(^2P_{3/2})$ photofragments are populated in the $|m|=1/2$ states only, and are described by $a_0^{(2)}(\perp)=-0.8$ [see Eq. (7)], which, to a first approximation, agrees well at all wavelengths with the measured $a_0^{(2)}(\perp)$.

The small deviation from $\beta=-1$ likely originates from about 3% excitation to the $B\,^3\Pi(0_u)^+$ state via a parallel transition. This state also produces $|m|=1/2$ only, therefore there is no deviation from $a_0^{(2)}(\perp)=-0.8$ from excitation to this state. In contrast, excitation or nonadiabatic transfer to the $A\,^3\Pi_u(1_u)$ state produces iodine atoms with equal population in the $|m|=3/2$ and $|m|=1/2$ states [Eq. (4)], giving an alignment of $a_0^{(2)}(\perp)=0$ for that state. Therefore, the average

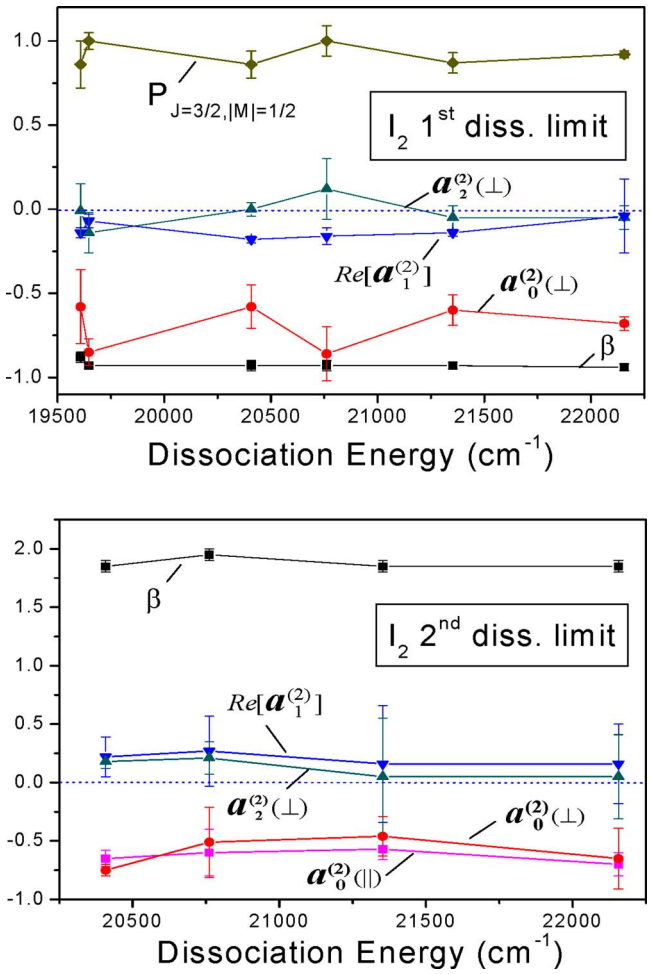

FIG. 3. Polarization parameters (values selected from Tables I and II) plotted as a function of the dissociation laser energy. The upper panel contains information extracted from the angular distribution of second largest ring in Fig. 2, corresponding to the first dissociation limit, $I(^2P_{3/2})+I(^2P_{3/2})$ at $\sim$12 400 cm^{-1}. The lower panel contains information extracted from the angular distribution of smallest ring in Fig. 2, corresponding to photodissociation of $X(v=0)$ to the second dissociation limit, $I(^2P_{3/2})+I(^2P_{1/2})$ at $\sim$20 000 cm^{-1}, for data at 20 408 and 20 761 cm^{-1}, and for the average of all vibrational states at the higher dissociation energies.

value of the $a_0^{(2)}(\perp)$ parameter will range between 0 and -0.8, and can be expressed in terms of the nonadiabatic transfer probability to the $A\,^3\Pi_u(1_u)$ state p by

$$a_0^{(2)}(\perp) = -\tfrac{4}{5}[1-p]. \tag{9}$$

As the value of the $a_0^{(2)}(\perp)$ parameter is within our error limits of -0.8, we can only put an upper limit on the transfer probability of about 25% (and it is likely much less than 25%). In addition, such nonadiabatic transfer would produce a nonzero value for the $a_2^{(2)}(\perp)$ parameter, given by[37]

$$a_2^{(2)}(\perp) = -\tfrac{4}{5}\sqrt{3/2}\sqrt{p(1-p)}\cos\Delta\varphi, \tag{10}$$

where $\Delta\varphi$ is the phase difference between the asymptotic wave functions associated with the $^1\Pi_u(1_u)$ and $A\,^3\Pi_u(1_u)$ states. The value of the $a_2^{(2)}(\perp)$ parameter is, however, measured to be zero (within the error limits) and the upper limit of p is only about 2% [as determined from the $a_2^{(2)}(\perp)$ parameter].

Therefore, we conclude that to a good approximation ($>95\%$) the first dissociation channel can be described by perpendicular excitation to the $^1\Pi_u(1_u)$ state, followed by adiabatic dissociation to yield $I(^2P_{3/2})$ photofragments characterized by $|m|=1/2$ with respect to the recoil direction. Any interference between the parallel and perpendicular transitions becomes evident in the $\mathrm{Re}[\boldsymbol{a}_1^{(2)}]$ and $\mathrm{Im}[\boldsymbol{a}_1^{(1)}]$ parameters; this interference is small because the magnitude of the parallel transition to the $B\,^3\Pi(0_u)^+$ state is about 3%, and therefore the $\mathrm{Re}[\boldsymbol{a}_1^{(2)}]$ and $\mathrm{Im}[\boldsymbol{a}_1^{(1)}]$ parameters are limited to about a third of their maximal value. The $\mathrm{Im}[\boldsymbol{a}_1^{(1)}]$ parameter [proportional to $\sin\Delta\varphi_{\parallel,\perp}$, where $\Delta\varphi_{\parallel,\perp}$ is the asymptotic phase difference between the wave functions associated with the $B\,^3\Pi(0_u)^+$ and $^1\Pi_u$ states] is measured to be zero. In comparison, the $\mathrm{Re}[\boldsymbol{a}_1^{(2)}]$ parameter (proportional to $\cos\Delta\varphi_{\parallel,\perp}$) is measured to be at most a third of its maximal value. We conclude that $\Delta\varphi_{\parallel,\perp}$ is approximately 0 or π.

We next consider the second dissociation channel (Table II), which yields a ground-state and spin-orbit excited iodine atoms,

$$I_2 \xrightarrow{h\nu} I(^2P_{3/2}) + I(^2P_{1/2}). \tag{11}$$

This channel is produced predominantly by parallel excitation (notice that β is close to +2 in Table II and Fig. 3) from the ground state to the $B\,^3\Pi(0_u)^+$ state. As mentioned above, this state correlates to atoms in the $|m|=1/2$ states only, producing $\boldsymbol{a}_0^{(2)}(\parallel)=-4/5$. The experimental data agrees, within error, with this value over all the photodissociation wavelengths and parent vibrational states (Table II), indicating that dissociation from this state is also adiabatic. The small contribution from a perpendicular transition (between about 2% and 5%), that causes the β parameter to be less than 2, originates from excitation to the $^1\Pi_u(1_u)$ state followed by nonadiabatic transfer to one of the $^3\Sigma_{1u}^+(1_u)$ states at large internuclear separation. During this process, the m-state distribution does not change, and thus we expect $\boldsymbol{a}_0^{(2)}(\perp)=-4/5$ and $\boldsymbol{a}_2^{(2)}(\perp)=0$, as for adiabatic dissociation from the $^1\Pi_u(1_u)$ state. It should be noted that despite the small contribution of the perpendicular component, the polarization of this channel can be observed because slice imaging [with the photolysis linear polarization parallel to the time-of-flight (TOF) axis] completely removes the contribution of the parallel transition in this geometry (in the limit of perfect slice imaging). The obtained values of $\boldsymbol{a}_0^{(2)}(\perp)$ and $\boldsymbol{a}_2^{(2)}(\perp)$ are within error of the expected ones.

Both dissociation pathways of I_2 were observed to proceed adiabatically, following excitation to the $B\,^3\Pi(0_u)^+$ and $^1\Pi_u(1_u)$ states. This adiabatic behavior extends to at least 10 000 cm^{-1} above the first dissociation limit and was followed to more than 2000 cm^{-1} above the second dissociation limit. Adiabatic behavior was also observed (at one dissociation energy) for Br_2.[30] In contrast, the dissociation of Cl_2 via the $C\,^1\Pi_u(1_u)$ state includes an additional nonadiabatic transfer to the $A\,^3\Pi_u(1_u)$ state (approximately 40%).[4,30] The situation is more complex for heteronuclear systems due to their lower symmetry, as was shown previously by Wouters *et al.*[8] for BrCl. For the simpler dihalogens we see that, as expected, the heavier systems dissociate adiabatically, whereas the lighter Cl_2 system shows significant nonadiabatic dissociation dynamics.

In a theoretical paper by Asano and Yabushita, it was concluded that the nonadiabatic transition probability between the dominant potential-energy surfaces of a molecule is influenced mainly by the spin-orbit splitting energy, the size of the atomic orbitals, and the relative nuclear velocity. According to their results, dihalogens with bigger spin-orbit splitting energy show more adiabatic behavior. This is consistent with the sequence Cl_2, Br_2, and our present experimental results on I_2. Our results could also be used to probe the dependence on the nuclear velocity (i.e., initial vibrational energy). We observe no distinct differences in polarization parameters for the vibrational states $v=0-3$, but this range of quantum numbers may be too small to expect a measurable effect.

ACKNOWLEDGMENTS

Financial support of this work by the Netherlands Organization for Scientific Research (NWO) under the programs NWO (FOM-MAP) and NWO Russia-Netherlands Cooperative Research Grant 047.009.001 is gratefully acknowledged. The participating groups are also grateful to the Commission of the European Communities for funding via the IHP Network HPRN-CT-2002-00183 and Laserlab-Europe Contract No. RII3-CT-2003-506350.

[1] R. N. Zare and D. R. Herschbach, Proc. IEEE **51**, 173 (1963).
[2] L. D. A. Siebbeles, M. Glass-Maujean, O. S. Vasyutinskii, J. A. Beswick, and O. Roncero, J. Chem. Phys. **100**, 3610 (1994).
[3] A. S. Bracker, E. R. Wouters, A. G. Suits, Y. T. Lee, and O. S. Vasyutinskii, Phys. Rev. Lett. **80**, 1626 (1998).
[4] A. S. Bracker, E. R. Wouters, A. G. Suits, and O. S. Vasyutinskii, J. Chem. Phys. **110**, 6749 (1999).
[5] T. P. Rakitzis, A. S. Kandel, A. Alexander, Z. H. Kim, and R. N. Zare, Science **281**, 1346 (1998).
[6] T. P. Rakitzis and R. N. Zare, J. Chem. Phys. **110**, 3341 (1999).
[7] G. G. Balint-Kurti, A. J. Orr-Ewing, J. A. Beswick, A. Brown, and O. S. Vasyutinskii, J. Chem. Phys. **116**, 10760 (2002).
[8] E. R. Wouters, M. Beckert, L. J. Russell, K. N. Rosser, A. J. Orr-Ewing, M. N. R. Ashfold, and O. S. Vasyutniskii, J. Chem. Phys. **117**, 2087 (2002).
[9] D. W. Chandler and P. L. Houston, J. Chem. Phys. **87**, 1445 (1987).
[10] A. T. J. B. Eppink and D. H. Parker, Rev. Sci. Instrum. **68**, 3477 (1997).
[11] R. N. Dixon, J. Chem. Phys. **85**, 1866 (1986).
[12] M. Mons and I. Dimicoli, J. Chem. Phys. **90**, 4037 (1989).
[13] T. P. Rakitzis, S. A. Kandel, A. J. Alexander, Z. H. Kim, and R. N. Zare, J. Chem. Phys. **110**, 3351 (1999).
[14] C. R. Gebhardt, T. P. Rakitzis, P. C. Samartzis, V. Ladopoulos, and T. N. Kitsopoulos, Rev. Sci. Instrum. **72**, 3848 (2001).
[15] D. A. Chestakov, S.-M. Wu, G. Wu, D. Parker, A. T. J. B. Eppink, and T. N. Kitsopoulos, J. Phys. Chem. A **108**, 8100 (2004).
[16] R. S. Mulliken, J. Chem. Phys. **55**, 288 (1971).
[17] K. P. Huber and G. Herzberg, *Constants of Diatomic Molecules* (Van Nostrand Reinhold, New York, 1970).
[18] J. Comes, U. Nielsen, and W. H. Schwarz, J. Chem. Phys. **58**, 2230 (1973).
[19] P. Venkateswarlu, Can. J. Phys. **48**, 1055 (1970).
[20] T. Readly, D. A. Beattie, M. C. R. Cockett, K. P. Lawley, and R. J. Donovan, Phys. Chem. Chem. Phys. **4**, 1398 (2002).
[21] J. A. Myer and J. A. Samson, J. Chem. Phys. **52**, 716 (1970).
[22] J. Tellinghuisen, J. Chem. Phys. **58**, 2821 (1971).
[23] J. Tellinghuisen, Chem. Phys. Lett. **49**, 485 (1977).
[24] J. Tellinghuisen, J. Chem. Phys. **76**, 4736 (1982).
[25] J. Tellinghuisen, Chem. Phys. Lett. **99**, 373 (1983).

[26] J. Tellinghuisen, J. Chem. Phys. **106**, 1305 (1996).
[27] M. Wu and P. M. Jonson, J. Chem. Phys. **90**, 74 (1989).
[28] A. Kvaran, H. Wang, G. H. Johannesson, and A. J. Yencha, Chem. Phys. Lett. **222**, 436 (1994).
[29] M. C. R. Cockett, D. A. Beattie, N. A. Macleod, K. P. Lawley, T. Ridley, and R. J. Donovan, Phys. Chem. Chem. Phys. **4**, 1419 (2002).
[30] T. P. Rakitzis and T. N. Kitsopoulos, J. Chem. Phys. **116**, 9228 (2002).
[31] E. Wrede, S. Laubach, S. Schulenburg, A. Brown, E. R. Wouters, A. J. Orr-Ewing, and M. R. N. Ashfold, J. Chem. Phys. **114**, 2629 (2001).
[32] Y. Asano and S. Yabushita, Chem. Phys. Lett. **372**, 348 (2003).
[33] H. Okabe, *Photochemistry of Small Molecules* (Wiley, New York, 1978).
[34] R. N. Zare, *Angular Momentum* (Wiley, New York, 1988).
[35] T. P. Rakitzis, A. J. van den Brom, and M. H. M. Janssen, Chem. Phys. Lett. **372**, 187 (2003).
[36] A. J. Orr-Ewing and R. N. Zare, Annu. Rev. Phys. Chem. **45**, 315 (1994).
[37] Reference 30. Notice the sign error in this equation.